Surface roughness prediction and optimization in the REMF process using an integrated DBN-GA approach

Junghee - Lee
Yun-Su - Seo
Jae-Seob Kwak (jskwak5@pknu.ac.kr)
Pukyong National University - Daeyeon Campus: Pukyong National University

Research Article

Keywords: Surface roughness prediction, Rotational Electro-Magnetic Finishing, Hierarchical neural structure, Deep belief network, Genetic algorithm

Posted Date: March 8th, 2022

DOI: https://doi.org/10.21203/rs.3.rs-1402070/v1

Surface roughness prediction and optimization in the REMF process using an integrated DBN-GA approach

Author : Jung-Hee Lee[1] · Yun-Su Seo[1] · Jae-Seob. Kwak[1]
[1]Department of Mechanical Engineering, Pukyong National University, Busan, 48547, Korea
Correspondence to: Jae-Seob Kwak jskwak5@pknu.ac.kr

Abstract

Surface roughness is a crucial factor affecting the surface quality of workpieces in the manufacturing industries. Thus, it is important to provide an accurate performance of surface roughness prediction and optimal parameters to reduce the burden of time and costs during the process. In this study, two predict models, namely multiple linear regression and deep belief network(DBN) models, were performed to accurately predict change in surface roughness in the rotational-electro magnetic finishing(REMF). Compared to the statistical-based model, the data-driven model based on the DBN architecture was a significantly considerable effect on surface roughness prediction in the REMF process. Among the considered DBN models, DBN5 architecture as [7, 14, 14, 1] showed effective features of the non-linear relationship between process parameters and response with the highest determination coefficient(R^2) of 0.9340 and the lowest mean squared error(MSE) of 1.3037×10^{-3} in the testing datasets. In addition, a genetic algorithm(GA) as a heuristic optimization technique was adopted to optimize the input parameters of the best derived DBN model. As a result, it proved that the DBN model integrated GA was able to be adopted for the accurate prediction of surface roughness and process optimization.

Keywords Surface roughness prediction · Rotational Electro-Magnetic Finishing · Hierarchical neural structure · Deep belief network · Genetic algorithm

1. Introduction

Recently, with the fast-growing requirements to improve surface integrity and functional performance in the ultra-precision engineering fields, the superior surface quality of manufactured components is in great demand. Surface roughness is one of the aspects of surface quality assessment that significantly affects the reliability, durability, wettability, reflection, and friction of products. Hence, a number of researchers are making considerable efforts to develop surface finishing technologies to improve surface roughness [1-3]. Traditional finishing processes are applied in a wide range of industries in practice. However, it still faces inherent limits in terms of surface defects and uneven surface finish, especially in complicated geometries. In the current manufacturing field, the latest research shows a trend away from traditional finishing methods towards advanced capabilities to achieve high surface finishing performance for micro-sized components having a complex shape. Magnetic energy-assisted finishing processes have proven effective for ultra-smooth surface among the advanced finishing technologies in the last few decades, where multiple cutting edges of tools with controllable magnetic force are able to obtain a high degree of micro/nano surface finishing performance [4,5].

Numerous studies of magnetic surface finish have been extensively conducted from diverse points of view to develop process efficiency and establish a predictive model representing a relationship between process parameters and surface roughness improvement. Singh and Singh simulated magnetic flux density in magnetorheological finishing(MRF) operation to determine a theoretically optimized experimental setup that enabled magnetic intensity on the external surface of conical-shaped material to be uniform. Based on the simulated approach, a theoretical surface roughness model and optimal condition for the fine surface finish were established. In addition, actual experiments at the optimal condition were carried out to the validated predictive model. It was concluded that the suggested MRF method was adequate for improving micrometric surface characteristics on the conducted materials [6]. Sirwal et al. developed magnetic-assisted tools that can perform reciprocating and rotational motion to achieve high surface quality with tight tolerance for the cylindrical blind surface in the MRF process. Based on the response surface methodology(RSM), researchers made an effort to analyze the influences of process parameters on better surface characteristics and to derive a mathematical statistical model of finished surface variation. In experimental and statistical analysis, finishing efficiency was dominantly determined by rotational speed, and surface roughness of the conducted areas improved by 85% at the optimal condition. Furthermore, the error rate of the predictive model was less than 10% compared to the experimental work. Thus, it was said that the derived model for surface roughness improvement was quite reliable [7]. Nagdeve et al. obtained precise surface of an intricate implant by adopting rotational magnetorheological abrasive flow finishing(MAFF) with the help of a special fixture that maintained constant abrasive velocity and magnetic field intensity in the finishing zone. To provide a predictive model of surface improvement and to optimize input variables, RSM as a statistical analysis was employed. The results showed that surface quality improved by 73% with less time compared to the previous MAFF process [8]. Misra et al. established theoretical models by applying a genetic algorithm to fulfill multi-objective optimization in terms of

maximum surface roughness improvement and minimum material loss in the ultrasonic-assisted magnetic abrasive finishing(MAF) process. In order to validate optimized models, linear regression models were given from the experimental approach based on a Taguchi orthogonal array method. Consequently, the findings indicated that the results obtained from confirmatory experiments were in good agreement with the theoretical model [9]. Ahmad et al. applied the MAF process with various diametric sintering magnetic abrasives to improve the capability for micrometric surface finish. Based on experimental observations, the statistical models for the ratio of change in surface roughness were derived. It clearly showed that the trend of both results was quantitative similar [10]. Although the mathematical models for surface roughness prediction by regression analysis are widely available, it is impractical to accurately describe the complex non-linearity of the processes due to uncontrollable factors that influence the relative motion between the workpiece surface and flexible tools [11-13].

With the development of computer technologies, artificial neural networks(ANNs) have become more popular as a robust predictive strategy to accurately establish the non-linear relationship between input variables and respond, unlike the statistical model. Deep neural network(DNN), which is one of the supervised learning models in the ANNs, is commonly used and has demonstrated outstanding predictive ability. Thus, in the literature, a number of researchers attempt to build predictive models of surface roughness to capture complex nonlinear relationships. Peng et al. presented a cutting force model based on the both linear regression and DNN methodologies. Consequently, the DNN-based model yielded exceptional performance rather than the existing model [14]. Ahmad et al. developed a DNN-based model for tri-objective models in terms of change in surface roughness, microhardness, and modulus of elastic indentation for Ti-6Al-4V material in the MAF process. Moreover, a genetic algorithm(GA) was employed for optimizing the system. As a result, the combined DNN-GA-based model was recommended to obtain suitable output in comparison with the experimental trials [15]. Singh et al. introduced an ANN-MFO learning algorithm in the MAF process to improve final surface integrity and optimize process parameters. The effectiveness of this hybrid methodology was successfully verified with a minimum error rate [16]. Kooialippor et al. made a predictive model for the performance assessment of the penetration rate of a tunnel boring machine. In order to evaluate prediction performance between ANN and deep belief network(DBN) models, root mean square(RMSE) and coefficient of determination(R^2) were compared. Based on the results, this study was proved that DNN was a promising tool for prediction with a large amount of data [17]. Stojanović et al. used the DNN for predicting friction coefficient and wear rate on hybrid aluminum matrix composites. From the observation of this study, the accuracy performance of the predictive model driven by the DNN was similar to the experimental verification with 99% [18]. Despite success of the effective prediction, DNN still experiences difficulties in terms of local minima, gradient vanishing, and slow convergence rate. In order to address these limitations, the DBN with hierarchical structures has attracted attention as a promising tool in current studies and practice.

This study established two types of predictive models driven by multiple linear regression and hierarchical DBN models for providing an accurate predictive model for surface roughness of stainless steel(SS)316 in the rotational electro-magnetic finishing(REMF) process. To train both models, a total of 72 experiments were carried out by the mixed-level orthogonal array $L_{18}(2^1x3^7)$ with 4 iterations. The best model showed the accurate prediction was selected by three statistical indicators, namely R^2, mean squared error(MSE) as the cost function, and F-test. In addition, a genetic algorithm was employed to define the optimal input parameters of the best predictive model.

2. Theoretical background of deep belief network

The DBN is a hierarchical neural network with stacked numerous restricted Boltzmann machines(RBMs). Therefore, in this chapter, the theoretical background of the RBMs as a basis of DBN is introduced in detail.

2.1 Restricted Boltzmann machine

RBM is an energy-based stochastic graphical model consisting of visible layer $\boldsymbol{v}$ with m neurons at the bottom and hidden layers $\boldsymbol{h}$ with n neurons at the top, as shown in Fig. 1. In the RBM structure, neurons in the adjacent layers are fully connected by symmetric weight $\boldsymbol{w}$ without intralayer connection. Due to the independence of neurons, this data-driven method enables simplifying the training process and improving training efficiency. There are two types of RBM, called Bernoulli-Bernoulli RBM and Gaussian-Bernoulli RBM dependent upon data distribution of the visible neurons.

2.1.1 Bernoulli -Bernoulli RBM

Bernoulli-Bernoulli RBM consists of binary states $\boldsymbol{v} \in \{0,1\}^m$ in the visible layer and stochastic binary features $\boldsymbol{h} \in \{0,1\}^n$ in the hidden layer extracted from the visible units. The energy function for a joint configuration $(\boldsymbol{v}, \boldsymbol{h})$ in the Bernoulli-Bernoulli RBM could be expressed as follows.

$$E(\boldsymbol{v},\boldsymbol{h};\boldsymbol{\theta}) = -\boldsymbol{v}^T\boldsymbol{w}\boldsymbol{h} - \boldsymbol{a}^T\boldsymbol{v} - \boldsymbol{b}^T\boldsymbol{h}$$

$$= -\sum_{i=1}^{m}\sum_{j=1}^{n} w_{ij}v_i h_j - \sum_{i=1}^{m} v_i a_i - \sum_{j=1}^{n} h_j b_j \tag{1}$$

where $\boldsymbol{v}$ is a visible vector $\boldsymbol{v} = \{v_1, v_2, \cdots, v_m\} \subset \{0,1\}$, v_i is the i^{th} visible variable, $\boldsymbol{h}$ is a hidden vector $\boldsymbol{h} = \{h_1, h_2, \cdots, h_m\} \subset \{0,1\}$, h_j is the j^{th} hidden variable, $\boldsymbol{w}$ denotes weight matrix which connects visible and hidden variables, w_{ij} is the weight connection between v_i and h_j, $\boldsymbol{a}$ and $\boldsymbol{b}$ are biases of visible and hidden nodes, respectively. $\boldsymbol{\theta}$ is $(\boldsymbol{a}, \boldsymbol{b}, \boldsymbol{w})$ as model parameters.

Given the energy function, the joint probability distribution over all neurons in the each layer is defined as follows.

$$p(\boldsymbol{v},\boldsymbol{h};\boldsymbol{\theta}) = \frac{1}{Z}\exp(-E(\boldsymbol{v},\boldsymbol{h};\boldsymbol{\theta})) \tag{2}$$

where Z is partition function or normalization constant, in which the variables of $p(\boldsymbol{v},\boldsymbol{h};\boldsymbol{\theta})$ is defined in range of [0, 1].
The marginal probability regarding the visible vector $\boldsymbol{v}$ is shown in Eq. (3).

$$p(\boldsymbol{v};\boldsymbol{\theta}) = \frac{1}{Z}\sum_{h}\exp(-E(\boldsymbol{v},\boldsymbol{h};\boldsymbol{\theta})) \tag{3}$$

In the training procedure of RBM, the model parameter $\boldsymbol{\theta}$ is optimized by stochastic gradient descent to maximize the log-likelihood of training data(input variables), which is corresponding to minimizing the energy function of the system. Log-likelihood function with a set of training data $T = \{v^1, v^2, \cdots, v^t\}, (t = 1, 2, \cdots, T)$ is defined as follows.

$$L(\boldsymbol{\theta}) = \sum_{t=1}^{T}\left[\log\sum_{h}\exp(-E(\boldsymbol{v},\boldsymbol{h};\boldsymbol{\theta})) - \log Z\right]$$

$$= \sum_{t=1}^{T}\left[\log\sum_{h}\exp(-E(\boldsymbol{v},\boldsymbol{h};\boldsymbol{\theta}))\right] - T\log Z \tag{4}$$

In order to update main parameters, the derivative of the log-likelihood with respect to weight, visible bias, and hidden bias should be calculated. Each derivative and updated parameter are expressed as following Eq. (5), Eq. (6), and Eq. (7).

$$\frac{\partial \log p(\boldsymbol{v};\boldsymbol{\theta})}{\partial w_{ij}} = \langle v_i h_j\rangle_{data} - \langle v_i h_j\rangle_{model}$$

$$\Delta w_{ij} = \varepsilon\left(\langle v_i h_j\rangle_{data} - \langle v_i h_j\rangle_{model}\right) \tag{5}$$

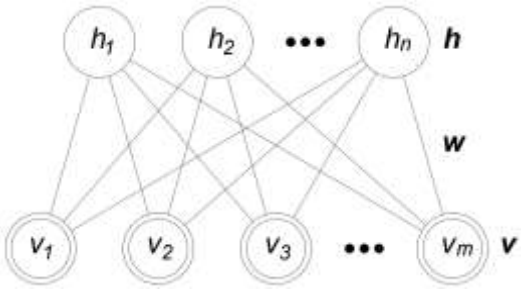

Fig. 1 Graphical structure of RBM

$$\frac{\partial \log p(\boldsymbol{v};\boldsymbol{\theta})}{\partial a_i} = \langle v_i \rangle_{data} - \langle v_i \rangle_{model}$$

$$\Delta a_i = \varepsilon(\langle v_i \rangle_{data} - \langle v_i \rangle_{model}) \tag{6}$$

$$\frac{\partial \log p(\boldsymbol{v};\boldsymbol{\theta})}{\partial b_j} = \langle h_j \rangle_{data} - \langle h_j \rangle_{model}$$

$$\Delta b_i = \varepsilon(\langle h_i \rangle_{data} - \langle h_i \rangle_{model}) \tag{7}$$

where $\langle \cdot \rangle_{data}$ is expectation computed over the given training data, $\langle \cdot \rangle_{model}$ is expectation over the distribution obtained from the resulting model, ε is a learning rate.
However, the latter term is computationally intractable. Thus, a contrast divergence(CD) algorithm as an approximation method with t iterations of Gibbs sampling, where $\langle \cdot \rangle_{model}$ is substituted for $\langle \cdot \rangle_t$ to calculate model distribution easily. Fig. 2 shows a stochastic procedure of t steps of Gibbs sampling. In the general RBM, one step of Gibbs sampling is suitable to acquire adequate values. Each neurons is independent, so the stochastic binary features of the hidden neurons $\boldsymbol{h}^{(0)}$ are determined by given visible variables $\boldsymbol{v}^{(0)}$. Relevant conditional probability term is given in Eq. (8)

$$p(h_j = 1|\boldsymbol{v};\boldsymbol{\theta}) = a\left(\sum_{i=1}^{m} w_{ij} v_i + b_j\right) \tag{8}$$

where $a(\cdot)$ is a sigmoid activation function.
In the next step, visible units $\boldsymbol{v}^{(1)}$ are reconstructed based on computed $\boldsymbol{h}^{(0)}$ by using following Eq. (9).

$$p(v_i = 1|\boldsymbol{h};\boldsymbol{\theta}) = a\left(\sum_{j=1}^{n} w_{ij} h_j + a_i\right) \tag{9}$$

2.1.2 Gaussian-Bernoulli RBM

In numerous practical applications, input variables as the visible neurons are real values rather than binary. Thus, Gaussian-Bernoulli RBM consisting of normalized data obtained from observed variables with Gaussian distribution and binary variables in the hidden layer is adopted instead of Bernoulli -Bernoulli RBM. The energy function for a joint configuration $(\boldsymbol{v}, \boldsymbol{h})$ in the Gaussian-Bernoulli RBM could be expressed as follows.

$$E(\boldsymbol{v}, \boldsymbol{h};\boldsymbol{\theta}) = -\sum_{i=1}^{m}\sum_{j=1}^{n} w_{ij} h_j \frac{v_i}{\sigma_i} - \sum_{i=1}^{m} \frac{(v_i - a_i)}{\sigma_i^2} - \sum_{j=1}^{n} h_j b_j \tag{10}$$

where σ_i denotes standard deviation related to visible neurons v_i.

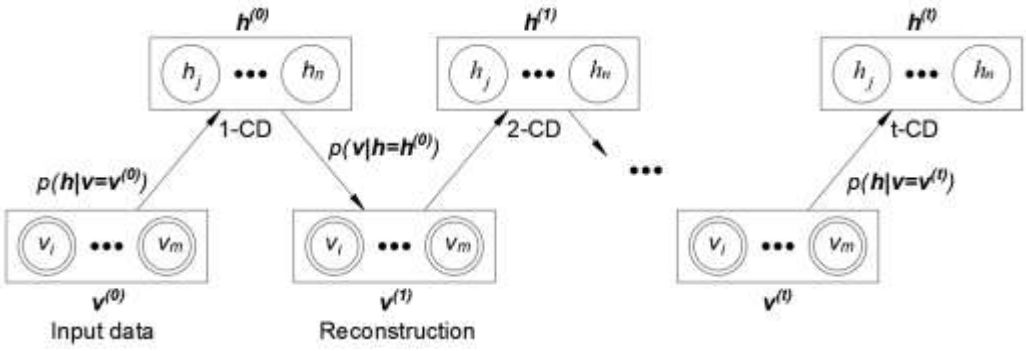

Fig. 2 Stochastic procedure of CD algorithm

Conditional probability of hidden and visible features is expressed as Eq. (11) and Eq. (12), respectively.

$$p(h_j = 1|\boldsymbol{v};\boldsymbol{\theta}) = \ a\left(\sum_{i=1}^{m} w_{ij}\frac{v_i}{\sigma_i^2} + b_j\right) \tag{11}$$

$$p(v_i = v|\boldsymbol{h};\boldsymbol{\theta}) = \ N\left(\boldsymbol{v}|\sum_{j=1}^{n} w_{ij}h_j + a_i, \sigma_i^2\right) \tag{12}$$

where $N(\cdot\,|\mu,\sigma_i^2)$ is a probability density function of the normal distribution with mean μ and standard deviation σ_i^2.

2.2 Deep belief network

The basic architecture of DBN consists of the multiple stacked RBM as shown in Fig. 3. There are two phases to train a DBN model, namely pre-training and fine-tuning algorithms.

In the pre-training step, a set of stacked RBMs is independently trained from the bottom to the top to initialize weights and biases layer by layer. Each trained hidden layer in the lower RBM is served as the visible layer in the next upper RBM. This unsupervised learning process is repeated until training for the last hidden layer is finished. After the upward training, the fine-tuning phase in which the model parameters are adjusted from top to bottom by means of supervised learning with a back-propagation algorithm is performed to minimize errors between output and the actual measurement.

The DBN model through these processes is determined by following joint probability distribution.

$$\begin{aligned} &P(\boldsymbol{v},\boldsymbol{h}^1,\boldsymbol{h}^2,\cdots,\boldsymbol{h}^{l-1},\boldsymbol{h}^l) \\ &= P(\boldsymbol{v}|\boldsymbol{h}^1)P(\boldsymbol{h}^1|\boldsymbol{h}^2)\cdots P(\boldsymbol{h}^{l-2}|\boldsymbol{h}^{l-1})P(\boldsymbol{h}^{l-1},\boldsymbol{h}^l) \end{aligned} \tag{13}$$

where l is the number of hidden layer in the DBN architecture.

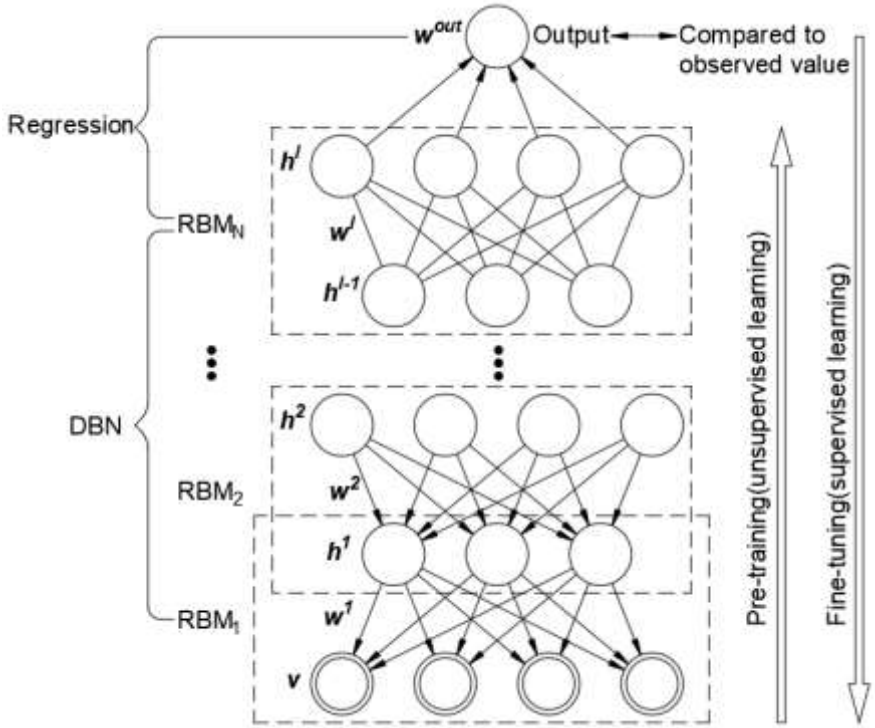

Fig. 3 Basic architecture of DBN model with regression analysis

Conditional probability distribution for $P(\boldsymbol{h}^i|\boldsymbol{h}^{i+1})$ can be obtained as Eq. (14).

$$P(\boldsymbol{h}^i|\boldsymbol{h}^{i+1}) = \prod_j P\left(h_j^i|\boldsymbol{h}^{i+1}\right)$$
$$P\left(h_j^i = 1|\boldsymbol{h}^{i+1}\right) = \sigma\left(b_j^i + \sum_j w_{ij}^{i+1} h_j^{i+1}\right),\ i = 0, 1, \cdots, l-2 \tag{14}$$

3. Experimental setup and DBN architecture

3.1 Principle of REMF operation

The REMF process is able to finish any complex geometries up to micro/nano-level surface finish. Fig. 4 showed the schematic drawing of the REMF process. It was separated into three parts dependent upon operating steps; a finishing area, a driving disc, and a controller. In the container as the finishing area, there were workpieces and a number of cylindrical-shaped abrasive particles with diluted water. On the application of the magnetic field induced by the driving disc embedded with permanent magnets, the abrasive particles not only aligned in the direction of the magnetic field but also started to experience an attractive force. Permanent magnets on the driving disc were alternatively arranged. When the driving disc was rotated by an AC motor as a part of the controller, the alternating magnetic field was induced. As a result, abrasives shown in Fig. 5 exhibited dynamic behavior that included radial and rotating motions laid along the direction of the magnetic field. The magnetic force and torque acting on the abrasives were represented as following Eq. (15) and Eq. (16), respectively.

$$F_p = md \cdot \nabla H = \chi V H \cdot \nabla H \tag{15}$$

$$T_p = md \times \nabla H = \chi V H \times \nabla H \tag{16}$$

where F_p and T_p were magnetic force and torque acting on the abrasive particle, m was magnetic pole, χ and V denoted susceptibility and volume of the abrasive particle, respectively, H was the magnetic field.
The dynamic motion induced by the magnetic energy generated kinetic energy, which improved surface roughness by colliding with the workpiece. Total kinetic energy acting on the abrasive particle was given as

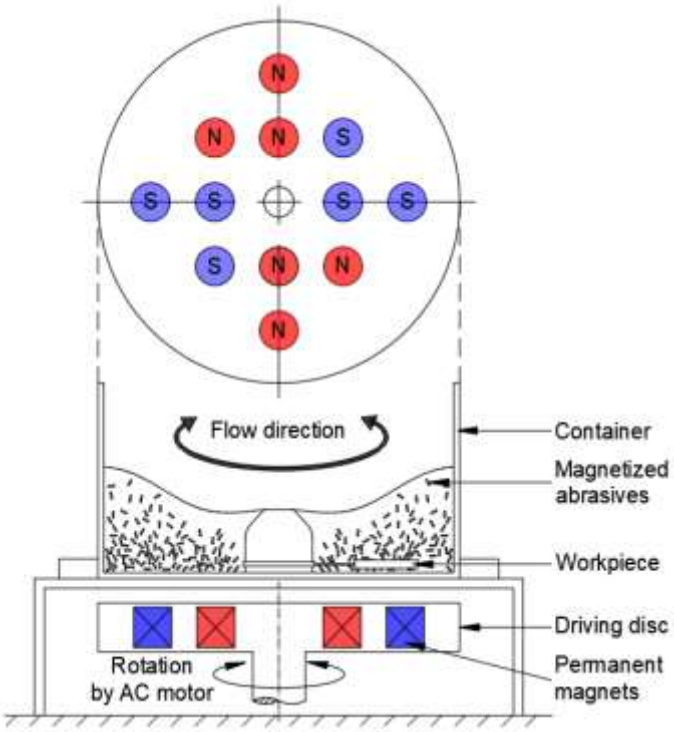

Fig. 4 Schematic drawing of REMF process

follows.

$$E_k = \frac{1}{2}\left(Mv^2 + Iw^2\right) \tag{17}$$

where M and v defined mass and velocity of abrasive particle, respectively, I was the moment of inertia, and w was angular velocity.

3.2 Experimental setup and measurement

The surface finishing performance in the REMF process was affected by magnetic and kinetic energy. As mentioned in section 3.1, the energy intensity was determined by the physical properties of the abrasive particles and rotating speed. Thus, six parameters as controllable factors, which included particle length, particle diameter, particle weight, diluted water quantity, rotational speed, and finishing time were selected as listed in Table 1.

Other fixed conditions were as follows. Fig. 6 showed external and internal views of an experimental device(SS370, Bhl) of the REMF process. The diameter of the finishing region was 370mm. In this study, the abrasive particles were cylindrical-shaped SS304, and the workpiece was SS316 plate in the dimensions of 50×35×5mm. The workpiece was placed at a radial distance of 65mm from the center, which measured a maximum magnetic flux density of 185mT. The diluted liquid was a mixture of compound and water at the volume ratio of 1:100 to help that abrasive particles were dispersed uniformly over the finishing region.

On the basis of the determined parameters with corresponding levels, mixed-level orthogonal array $L_{18}(2^1\times3^7)$ were established. Each combination for experiments was iterated four times. In order to investigate the effect of the REMF process on the surface finish of the SS316 workpiece, a quantitative measure of surface roughness R_a was evaluated by a stylus profilometer(SJ-301, Mitutoyo). A diamond stylus tip diameter of 2mm, the cut-

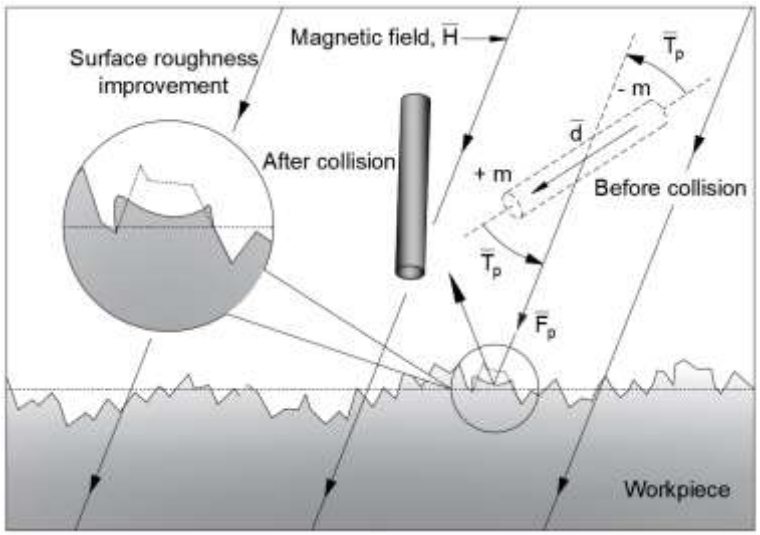

Fig. 5 Dynamic behavior of abrasive particle driven by magnetic force and torque

Table 1 Experimental factors and levels

Factor	Level		
	1	2	3
Particle length (mm), A	3.0	5.0	-
Particle diameter (mm), B	0.3	0.5	0.7
Particle weight (kg), C	1.0	1.4	1.8
Diluted water quantity (ℓ), D	1.0	2.0	3.0
Rotational speed (rpm), F	800	1,100	1,400
Finishing time (min), G	20	30	40

off value of 0.8mm, total measuring length of 4mm were designated for measurement. Fig. 7 illustrated measurement points selected in this study. Surface roughness at each point was measured ten times, and then three values that were close to the mean value were chosen to improve the accuracy of the measurement. Since the initial surface condition was not equal over all the workpieces, the ratio of change in surface roughness as a dimensionless coefficient was adopted for the assessment as given in Eq. (18).

$$\Delta SR_{Measure} = \frac{R_{a,initial} - R_{a,final}}{R_{a,initial}} \tag{18}$$

where $R_{a,initial}$ and $R_{a,final}$ were initial and final surface roughness, respectively.

3.3 DBN architecture

The predictive performance of the data-driven model was dependent upon network architecture. In this study, the architecture of DBN consisted of two sets of RBMs, where one visible layer and two hidden layers, with an additional regression layer as output with ReLU activation function. There were seven neurons corresponding to six process parameters designated in section 3.2 and $R_{a,initial}$ in the visible layer. Output layer for regression had one neuron represented as predictive $\Delta SR_{E,DBN}$. The number of the first visible neurons and the output neuron was set to be the same while the number of neurons in the hidden layers varies from {7, 14, 21}.

Total datasets for developing the predictive model were 72 obtained from experimentation. In order to improve the accuracy and reliability of the model, this study randomly divided 72 of whole data in the ratio of 5:1, which meant that 83% of the total, being 60 train datasets, was considered for network training and 17% of the total, being 12 test datasets, was used for model evaluation.

In the pre-training stage of $\Delta SR_{E,DBN}$ prediction, the input variables were preprocessed. Since the input variables were continuous data laid in different ranges and units, it needed to be normalized from 0 to 1. These numerical values were used as the visible units in the first step of RBM, so Gaussian-Bernoulli RBM was adopted as the first RBM structure to convert real values into binary stochastic variables for the next RBM training. A remaining structure of the DBN was Bernoulli-Bernoulli RBM. The initial weights at the beginning of the RBM were sampled from a Gaussian distribution with mean of 0 and standard deviation of 0.01. The biases were initialized to 0. The training ran for 1,000 epochs with a learning rate of 0.001. On the basis of the above information, the greedy layer-wise unsupervised training was carried out to obtain the network parameters in terms of weights and biases in each RBM structure.

When the pre-training was completely finished, initial parameters of the output layer on the top of the

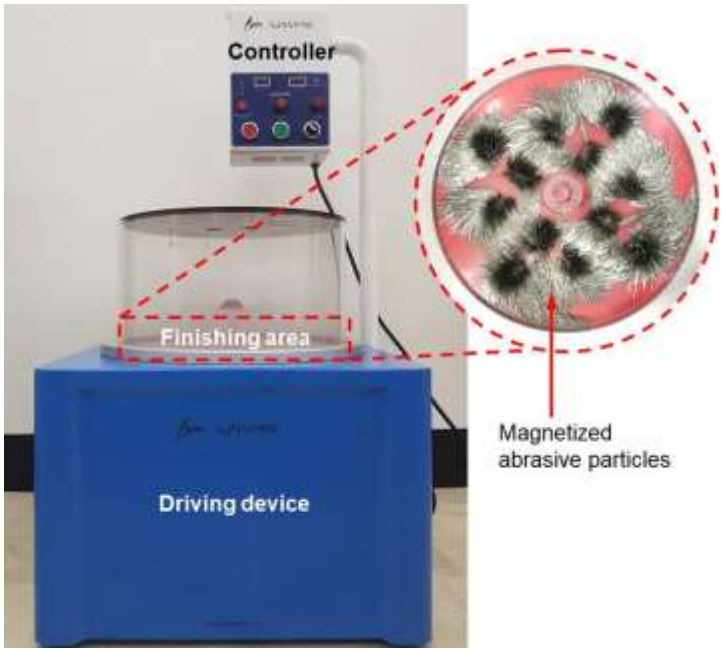

Fig. 6 External and internal view of experimental apparatus in REMF process

architecture and the model parameters derived from the unsupervised training were adjusted in a supervised manner with the back-propagation algorithm to minimize prediction error. An activation function of two sets of hidden layers and output layer were logistic sigmoid and ReLU, respectively. In order to accelerate convergence speed, Adam optimizer was introduced with a learning rate of 0.001. The epochs were set to 30,000 and an early stopping algorithm with 100 patiences was used to prevent underfitting and overfitting.

The performance of the predictive surface roughness model was evaluated with three statistical indicators, namely R^2, MSE as the cost function, and F-test.

4. Predictive model for surface roughness

4.1 Multiple linear regression model

Table 2 showed the calculated $\Delta SR_{Measure}$ of all experimental combinations in this study. Based on the experimental results, this section proposed predictive models with the help of statistical and deep learning approaches.

A multi regression model as the statistical analysis was an effective way of determining relationships between

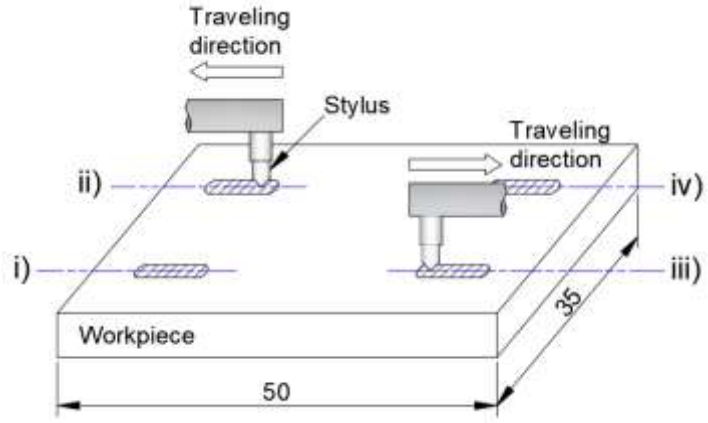

Fig. 7 Measurement method of surface roughness

Table 2 The ratio of change in surface roughness

Exp. no.	Factor and level						ΔSR_M			
	A	B	C	D	F	G	i)	ii)	iii)	iv)
1	1	1	1	1	1	1	0.1114	0.0514	0.1199	0.1554
2	1	1	2	2	2	2	0.1415	0.0602	0.2440	0.2060
3	1	1	3	3	3	3	0.0742	0.0882	0.2892	0.2301
4	1	2	1	1	2	2	0.1278	0.0758	0.5074	0.4334
5	1	2	2	2	3	3	0.1940	0.1547	0.4818	0.5229
6	1	2	3	3	1	1	0.0574	0.0692	0.1204	0.1422
7	1	3	1	2	1	3	0.1471	0.1317	0.2884	0.3218
8	1	3	2	3	2	1	0.1203	0.1425	0.3461	0.3071
9	1	3	3	1	3	2	0.2288	0.2149	0.4218	0.4067
10	2	1	1	3	3	2	0.1296	0.0547	0.1897	0.1625
11	2	1	2	1	1	3	0.0827	0.0926	0.0876	0.0805
12	2	1	3	2	2	1	0.0392	0.0691	0.1367	0.1692
13	2	2	1	2	3	1	0.0675	0.0556	0.2524	0.2383
14	2	2	2	3	1	2	0.1739	0.1100	0.1515	0.2101
15	2	2	3	1	2	3	0.0796	0.1176	0.2931	0.2929
16	2	3	1	3	2	3	0.0642	0.1211	0.4310	0.4491
17	2	3	2	1	3	1	0.1174	0.1098	0.3686	0.3687
18	2	3	3	2	1	2	0.1518	0.0829	0.1772	0.2099

independent and dependent variables. In order to predict $\Delta SR_{Pred,regression}$ in this study, second-order polynomial regression was employed as following Eq. (19).

$$\Delta SR_{Pred,regression} = \beta_0 + \sum_{i=1}^{6}(\beta_i x_i + \beta_{i+6} x_i^2) \tag{19}$$

where $\Delta SR_{Pred,regression}$ was the estimated response obtained from the second-order equation, β_0 and β_i were regression coefficients, x_1, x_2, x_3, x_4, x_5, and x_6 denoted normalized process parameters, which were particle length(A), particle diameter(B), particle weight(C), diluted liquid amount(D), rotational speed(F), working time(G), respectively.

Based on the experimental results, the second-order mathematical model for the ratio of change in surface roughness was given as follows.

$$\begin{aligned}\Delta SR_{Pred,regression} = {} & 0.0852 - 0.0485A + 0.1997B + 0.0531C \\ & - 0.0374D + 0.1873F \\ & + 0.1319G - 0.0887B^2 \\ & - 0.0750C^2 + 0.0077D^2 \\ & - 0.1001F^2 - 0.0743G^2\end{aligned} \tag{20}$$

The most dominant factor by comparing absolute values of coefficients was particle diameter, followed by rotational speed, working time, particle weight, particle length, and diluted liquid quantity.

In order to evaluate the performance of the developed regression model, three statistical indicators, namely R^2, MSE, and F-test were applied same as evaluation criteria for the DBN model. The R^2 had a high explanatory value of 0.9199 close to 1, which meant that there was a consistent agreement between predicted results and experimental data. The difference between predicted and observed values was defined as MSE. This model had a small value of 0.4432×10^{-3}, which was close to the best fit of 0. Fig. 8 showed residual plot with histogram for the multiple linear regression-based model. As can be seen, the residual had approximately constant variance and followed the normal distribution. Table 3 listed the results of analysis of variance(ANOVA). From the result of F-ratio, the regression model had reasonable accuracy with a confidence level of 95%. Therefore, it was said that it provided reliable prediction for change in surface roughness in the REMF process.

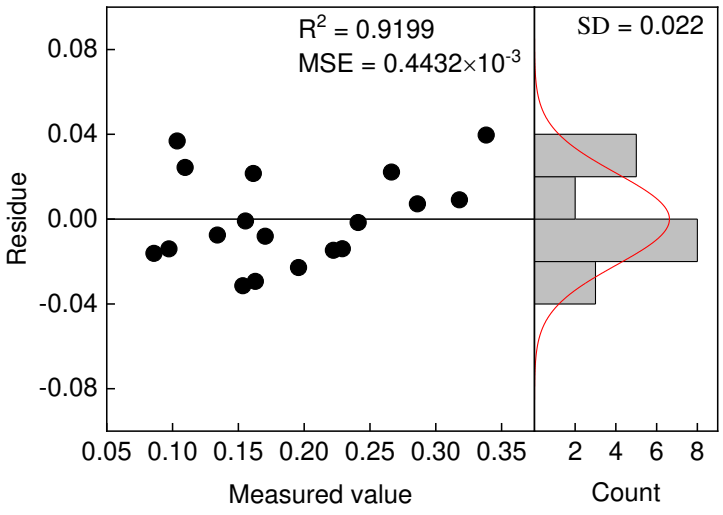

Fig. 8 Scatter plot and histogram regarding residues

Table 3 ANOVA for multiple linear regression model

Factor	SS	DOF	V	F_0
Regression	0.09166	11	0.00833	6.27*

Residue	0.00798	6	0.00133
Total	0.09964	17	

4.2 DBN model

Table 4 showed the average R^2 and MSE of the considered 9th DBN architecture in this study after 3 iterations of the training. As can be seen, the ranges of R^2 for training datasets and testing datasets were from 0.9787 to 0.9910 and from 0.8733 to 0.9340, respectively. Both values were significantly high and laid on the straight line, which indicated a good fit of the suggested hierarchal network model. In terms of MSE, the average MSE of testing datasets was 1.6581×10^{-3}, which was 5 times higher than training one of 0.3126×10^{-3}. This was because testing datasets as new data for the derived model based on the training ones were never used before. However, all values were low degree, so it could be concluded that the DBN model for prediction $\Delta SR_{Pred,DBN}$ in this study showed the excellent generalization capability to new samples. Among the architecture, DBN5 having 7-14-14-7 was the best predictive model with the minimum MSE of 1.3037×10^{-3} and maximum R^2 of 0.9340 in the testing datasets as shown in Fig. 9. From the results of ANOVA as listed in Table 5, the DBN5 models for training and testing datasets were statistically significant at 99% and 95% of confidence levels, respectively. Therefore, the derived model by mean of the DBN was sufficiently reliable for surface roughness prediction in the REMF process.

Table 4 Average R^2 and MSE results of DBN architectures

Architecture no.	Architecture (v- h_1-h_2-out)	Training datasets		Testing datasets	
		R^2	MSE($\times 10^{-3}$)	R^2	MSE($\times 10^{-3}$)
DBN1	7-7-7-1	0.9797	0.3078	0.8923	1.4884
DBN2	7-7-14-1	0.9837	0.3153	0.9027	1.8651
DBN3	7-7-21-1	0.9843	0.2486	0.8970	1.6912
DBN4	7-14-7-1	0.9870	0.8710	0.8733	2.3187
DBN5	7-14-14-1	0.9900	0.1518	0.9340	1.3037
DBN6	7-14-21-1	0.9860	0.2224	0.8747	1.4972
DBN7	7-21-7-1	0.9910	0.1493	0.8813	1.8786
DBN8	7-21-14-1	0.9850	0.2344	0.9087	1.5696
DBN9	7-21-21-1	0.9787	0.3127	0.9167	1.3106

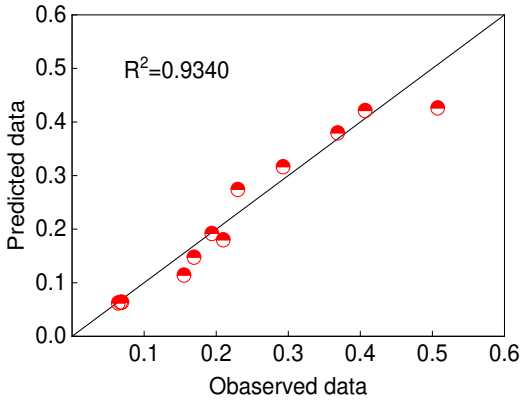

Fig. 9 Correlation between predicted and observed data for testing datasets in DBN5

Table 5 ANOVA for training and testing datasets in DBN5

DBN5	Factor	SS	DOF	V	F_0
Training datasets	Regression	0.86491	7	0.12356	2182.43**
	Residue	0.00294	52	0.00005	
	Total	0.86785	59		
Testing datasets	Regression	0.21424	7	0.03061	9.77*
	Residue	0.01253	4	0.00313	

	Total	0.22677	11

4.3 Comparison

In this study, two different types of prediction approaches, which were the traditional statistical model and the deep neural network model, were suggested to estimate the ratio change in surface roughness on SS316 in the REMF process. Table 6 presented calculated R^2 and MSE for each model. From the comparison of R^2 between both models, the values obtained from training and testing phases of the DBN5 model yielded 7% and 1.5% higher prediction performance, respectively compared to the multiple linear regression model. Fig. 10 showed the predictive values of both models against actual experimental results. As can be seen, the predictive value of DBN5 had less deviation compared with the multiple linear regression model. It was proved that the well-trained DBN model had a good agreement between observed and predicted data. In terms of MSE, all the values of both approaches, close to 0, were satisfactory for predicting surface roughness with high accuracy and reliability rate. Although the multiple linear regression model provided the low MSE of 0.443×10^{-3}, the predictive model was derived by mean value, which was the insufficient tool to predict non-linear characteristics.

5. Genetic algorithm optimization

Based on the training DBN model, it was found that the DBN5 architecture that consisted of 7 neurons of input variables, 14 neurons of each hidden layer, and 1 neuron of output. In order to improve the practical applicability of the REMF process, it was important to optimize the process parameters for the best ΔSR performance of the DBN5 model. In this study, GA as a heuristic optimization technique was applied to obtain the optimal solution.

GA involved five main stages, which included population initialization, selection, crossover, mutation, and evaluation. In the first stage, population randomly created 10 chromosomes having the binary state of 27 genes that contain characteristics of input parameters. Afterward, the best two chromosomes were selected by comparing ΔSR as a fitness function with tournament selection. From the superior chromosomes, offspring as a new solution was produced by exchanging a group of genes between the selected parameters in the crossover process. After the crossover operator, some of the genes in the offspring were randomly modified with a mutation rate of 0.01 to avoid local optima. The algorithm iterated 50 generations until finding out the best ΔSR. Fig. 11 illustrated the convergence curve toward maximizing ΔSR in the REMF process as the objective function during 50 generations. As can be seen, a trend of ΔSR increased sharply before 7 generations. After that convergence curve was stable and reached the maximum ΔSR of 0.530 at 25 generations. Table 7 listed the best combination of process parameters at the optimal condition. In comparison with the results of a Taguchi

Table 6 Statistical comparison between DBN5 and multiple linear regression models

Statistical criteria	Multiple linear regression	DBN5	
		Training datasets	Testing datasets
R^2	0.9199	0.9900	0.9340
MSE	0.4432	0.1518	1.3037

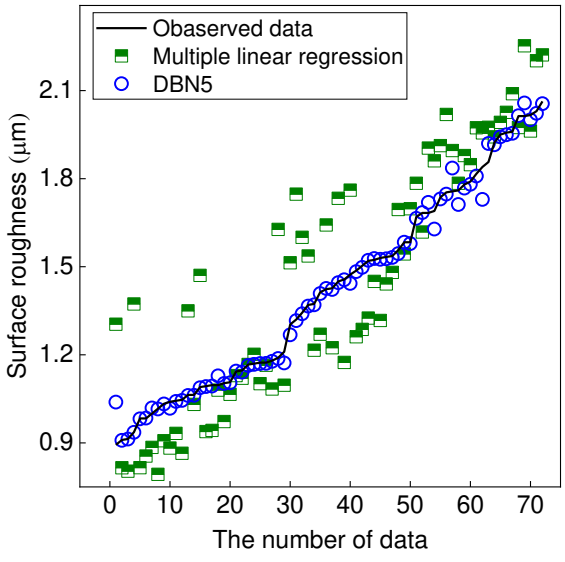

Fig. 10 Comparison between multiple linear regression model and DBN5 against observed data

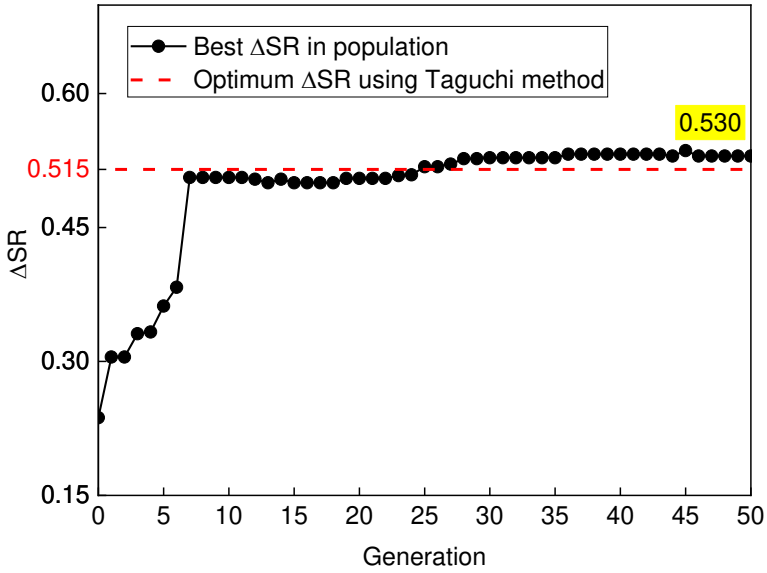

Fig. 11 Comparison of best ΔSR between the DBN5 integrated GA and Taguchi methods

Table 7 Optimal process parameters of the DBN5 integrated GA and Taguchi methods

Optimal strategy	Process parameters						
	A	B	C	D	F	G	$R_{a,initial}$
DBN5 integrated GA	3mm	0.7mm	1.3kg	1.0ℓ	1,323rpm	35min	2.478μm
Taguchi method	3mm	0.7mm	1.4kg	1.0ℓ	1,400rpm	30min	-

method, the convergence ΔSR of GA was close to that of the Taguchi strategy of 0.515. Thus, it proved that the DBN model integrated GA was able to be adopted for the accurate prediction of ΔSR and process optimization.

6. Conclusions

This study aimed to provide an accurate prediction model for surface roughness in the REMF process to improve surface quality. In order to develop the best predictive model well-explained non-linearity of the process, the statistical model based on the multiple linear regression and the data-driven model based on the DBN architecture were compared with three criteria which were R^2, MSE, and F-test. Based on the best model resulting from comparison, the GA algorithm was adopted to optimize the process parameters. The main observations of this study were summarized as follows.

- R^2 and MSE of the mathematical regression model were 0.9199 and 0.4432×10^{-3}, respectively. From the ANOVA, this model had the confidence level of 95%.
- From the developed 9th DBN architecture, the range of R^2 from the training datasets was from 0.9787 to 0.9910, which yielded about 7% higher prediction performance than the multiple linear regression model. The average MSE from the training datasets was 0.3126×10^{-3}, which was less than 30% compared to the statistical model. Therefore, it proved that the DBN model was practical to accurately predict the complex non-linear relationship between input and output variables in the process.

- Among the considered DBN structures, DBN5 achieved excellent prediction performance with R^2 of 0.9900 and MSE 0.1518×10^{-3} in the training datasets, and R^2 of 0.9340 and MSE 1.3037×10^{-3} in the testing datasets. In addition, training and testing datasets were statistically significant at 99% and 95% of confidence levels, respectively.
- From the comparison between the DBN5 and multiple linear regression model, DBN5 was close to actual experimental results. It meant that the well-trained model suggested in this study improved prediction accuracy and reliability for surface roughness in the REMF process.
- At the optimal input parameters of the DBN5 obtained from the GA algorithm, which were 3mm of particle length of 3mm, particle diameter of 0.7mm, particle weight of 1.3kg, liquid water quantity of 1.0 ℓ, rotational speed of 1,323rpm, working time of 35min, and initial surface roughness of 2.478 μm, maximum ΔSR was about 0.530.

Reference

[1] Prakash C, Singh S, Pramanik A, Basak A, Królczyk G, Bogdan-Chudy M, Wu YL, Zheng HY (2021) Experimental investigation into nano-finishing of β-TNTZ alloy using magnetorheological fluid magnetic abrasive finishing process for orthopedic applications. J of Materials Research and Technol 11:600-617. https://doi.org/10.1016/j.jmrt.2021.01.046

[2] Cao L, Sendur K (2019) Surface roughness effects on the broadband reflection for refractory metals and polar dielectrics. Materials 12(19):3090. https://doi.org/10.3390/ma12193090

[3] Arora K, Singh AK (2021) Theoretical and experimental investigation on surface roughness of straight bevel gears using a novel magnetorheological finishing process. Wear 476:203693. https://doi.org/10.1016/j.wear.2021.203693

[4] Ahmad S, Singari RM, Mishra RS (2020) Modelling and optimisation of magnetic abrasive finishing process based on a non-orthogonal array with ANN-GA approach. Transactions of the IMF 98(4):186-198. https://doi.org/10.1080/00202967.2020.1776966

[5] Xing B, Zou Y (2020) Investigation of finishing aluminum alloy A5052 using the magnetic abrasive finishing combined with electrolytic process. Machines 8(4):78. https://doi.org/10.3390/machines8040078

[6] Singh M, Singh AK (2021) Magnetorheological finishing of variable diametric external surface of the tapered cylindrical workpieces for functionality improvement. J. of Manuf Processes 61:153-172. https://doi.org/10.1016/j.jmapro.2020.10.074

[7] Sirwal SA, Singh AK, Paswan SK (2020) Experimental analysis of magnetorheological finishing of blind hole surfaces using permanent magnet designed tools. J of the Brazilian Society of Mech Sci and Eng 42(3):1-23. https://doi.org/10.1007/s40430-020-2225-6

[8] Nagdeve L, Jain VK, Ramkumar J (2020) Optimization of process parameters in nano-finishing of Co-Cr-Mo alloy knee joint. Materials and Manuf Processes 35(9):985-992. https://doi.org/10.1080/10426914.2020.1750633

[9] Misra A, Pandey PM, Dixit US, Roy A, Silberschmidt VV (2019) Multi-objective optimization of ultrasonic-assisted magnetic abrasive finishing process. Int J of Adv Manuf Technol 101(5):1661-1670. https://doi.org/10.1007/s00170-018-3060-0

[10] Ahmad S, Gangwar S, Yadav PC, Singh DK (2017) Optimization of process parameters affecting surface roughness in magnetic abrasive finishing process. Materials and Manuf Processes 32(15):1723-1729. https://doi.org/10.1080/10426914.2017.1279307

[11] Chen Y, Jin Y, Jiri G (2018) Predicting tool wear with multi-sensor data using deep belief networks. Int J of Adv Manuf Technol 99(5):1917-1926. https://doi.org/10.1007/s00170-018-2571-z

[12] Vasanth XA, Paul PS, Varadarajan AS (2020) A neural network model to predict surface roughness during turning of hardened SS410 steel. Int J of System Assurance Eng and Management 11(3): 704-715. https://doi.org/10.1007/s13198-020-00986-9

[13] Hao X, Guo T, Huang G, Shi X, Zhao Y, Yang Y (2020) Energy consumption prediction in cement calcination process: a method of deep belief network with sliding window. Energy 207:118256. https://doi.org/10.1016/j.energy.2020.118256

[14] Peng B, Bergs T, Schraknepper D, Klocke F, Döbbeler B (2019) A hybrid approach using machine learning to predict the cutting forces under consideration of the tool wear. Procedia Cirp 82:302-307. https://doi.org/10.1016/j.procir.2019.04.031

[15] Ahmad S, Singari RM, Mishra RS (2021) Tri-objective constrained optimization of pulsating DC sourced magnetic abrasive finishing process parameters using artificial neural network and genetic algorithm. Materials and Manuf Processes 36(7):843-857. https://doi.org/10.1080/10426914.2020.1866196

[16] Singh RK, Gangwar S, Singh DK, Pathak VK (2019) A novel hybridization of artificial neural network and moth-flame optimization (ANN–MFO) for multi-objective optimization in magnetic abrasive finishing of aluminium 6060. J of the Brazilian Society of Mechanical Sci and Eng 41(6):1-19.

https://doi.org/10.1007/s40430-019-1778-8
[17] Koopialipoor M, Tootoonchi H, Armaghani DJ, Mohamad ET, Hedayat A (2019) Application of Deep neural networks in predicting the penetration rate of tunnel boring machines. Bulletin of Engineering Geology and the Environment 78(8):6347-6360. https://doi.org/10.1007/s10064-019-01538-7
[18] Stojanović B, Vencl A, Bobić I, Miladinović S, Skerlić J (2018) Experimental optimisation of the tribological behaviour of Al/SiC/Gr hybrid composites based on Taguchi's method and artificial neural network. J of the Brazilian Society of Mech Sci and Eng 40(6):1-14. https://doi.org/10.1007/s40430-018-1237-y

Declarations

Funding No funding was received for conducting this study.

Conflicts of interest All authors declared they had no conflicts of interest.

Availability of data and material All the data supporting the results of this study were available within the article.

Ethics approval Not applicable

Consent to participate Not applicable.

Consent for publication All authors gave consent for publication.

Authors' contributions Lee JH and Seo YS performed experiments and data analysis. In addition, they contributed to writing the paper. Kwak JS supervised the project and reviewed the paper.

List of figures

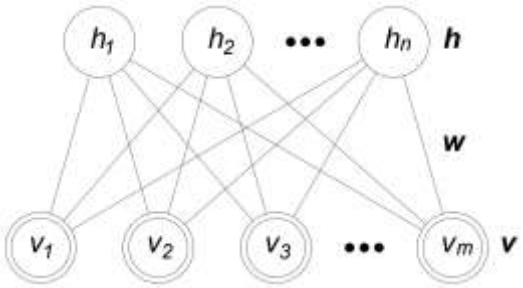

Fig. 1 Schematic structure of RBM

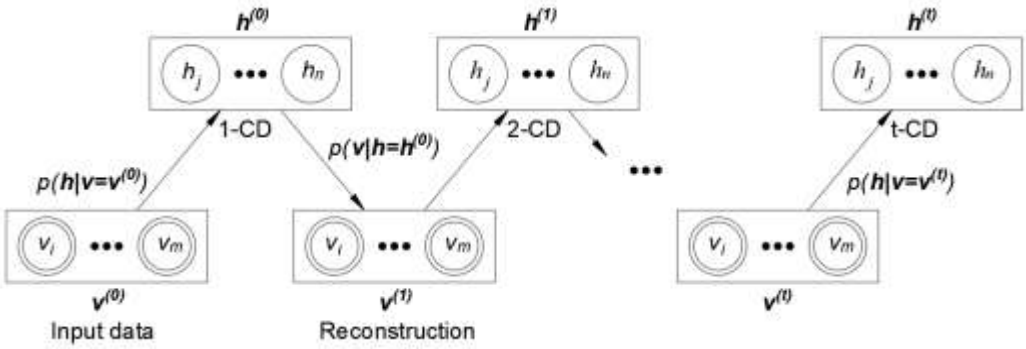

Fig. 2 Stochastic procedure of CD algorithm

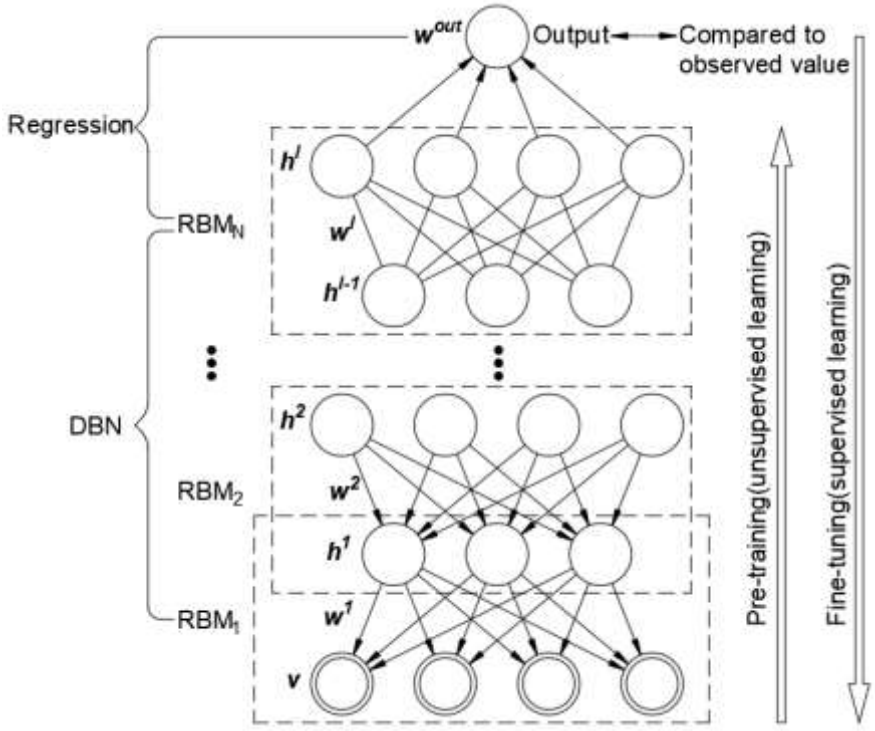

Fig. 3 Basic architecture of DBN model with regression analysis

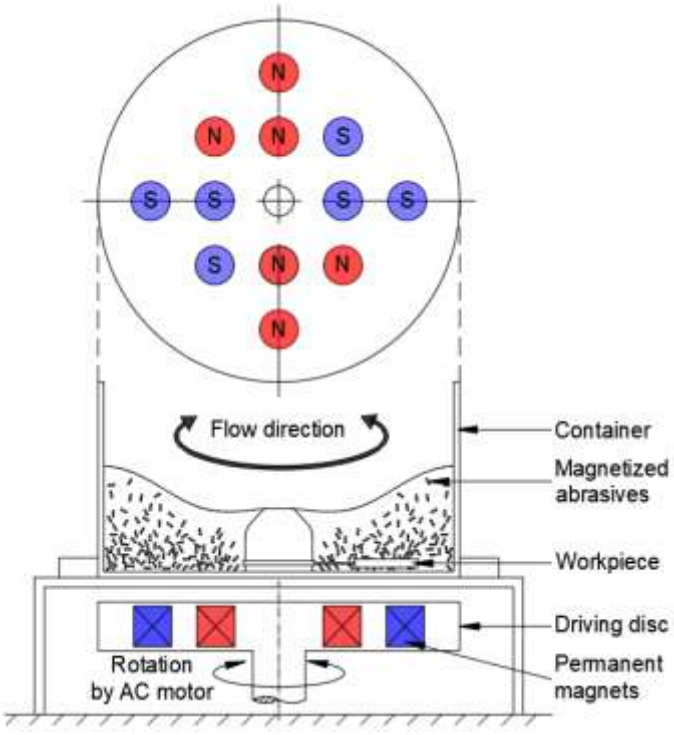

Fig. 4 Schematic drawing of REMF process

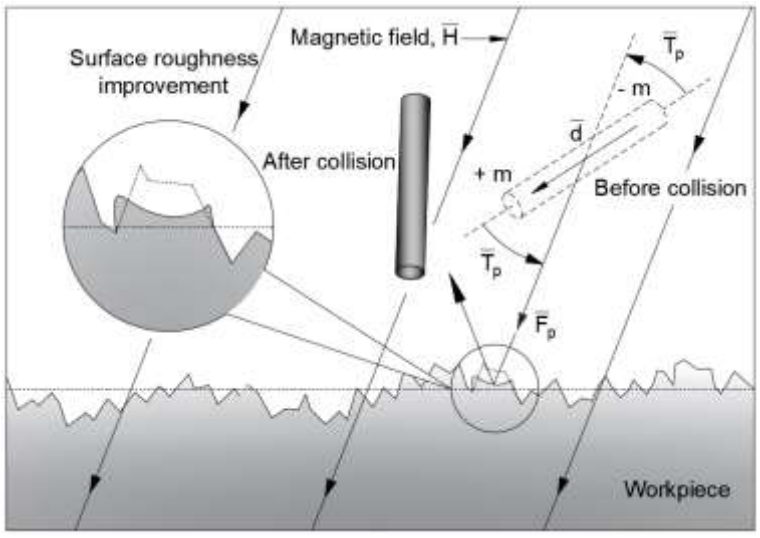

Fig. 5 Dynamic behavior of abrasive particle driven by magnetic force and torque

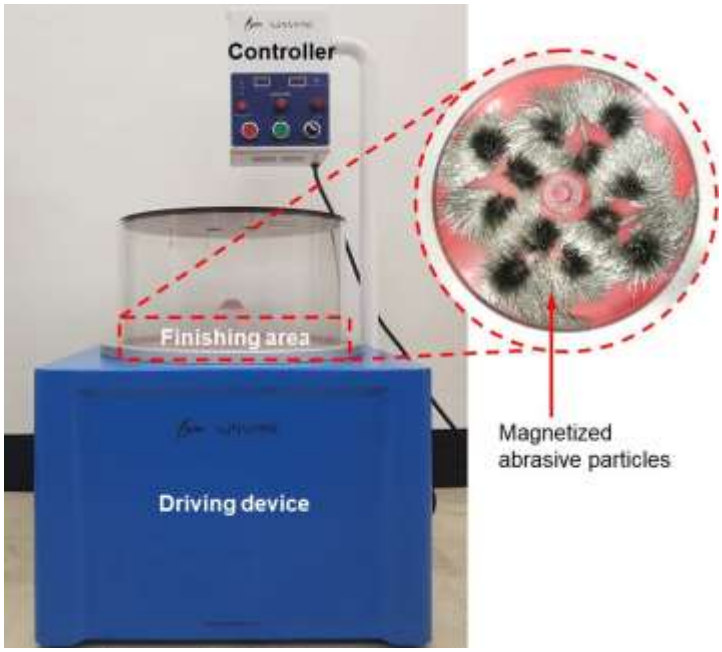

Fig. 6 External and internal view of experimental apparatus in REMF process

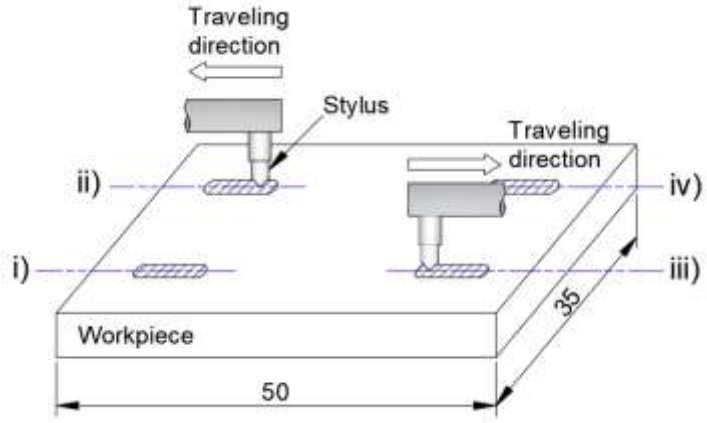

Fig. 7 Measurement method of surface roughness

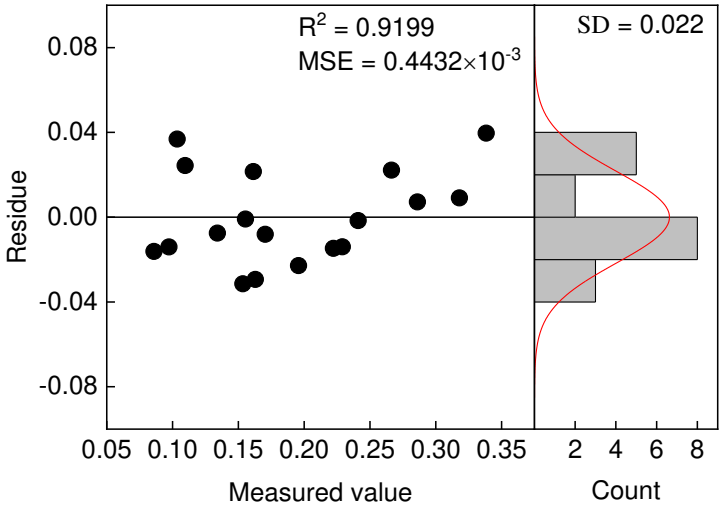

Fig. 8 Scatter plot and histogram regarding residues

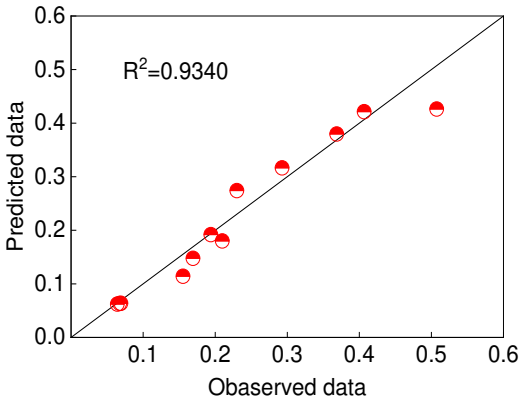

Fig. 9 Correlation between predicted and observed data for testing datasets in DBN5

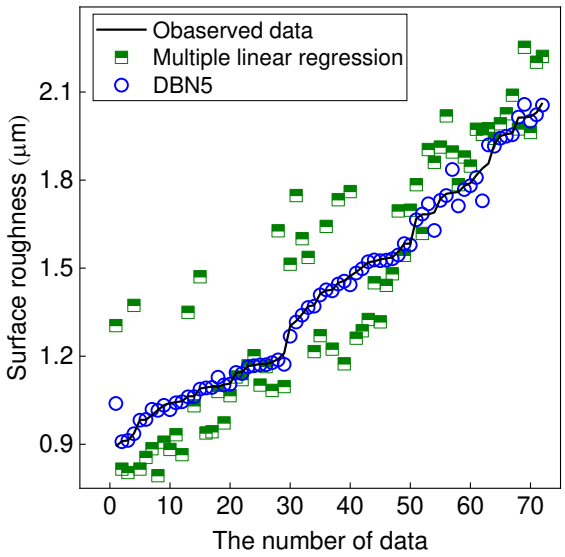

Fig. 10 Comparison between multiple linear regression model and DBN5 against observed data

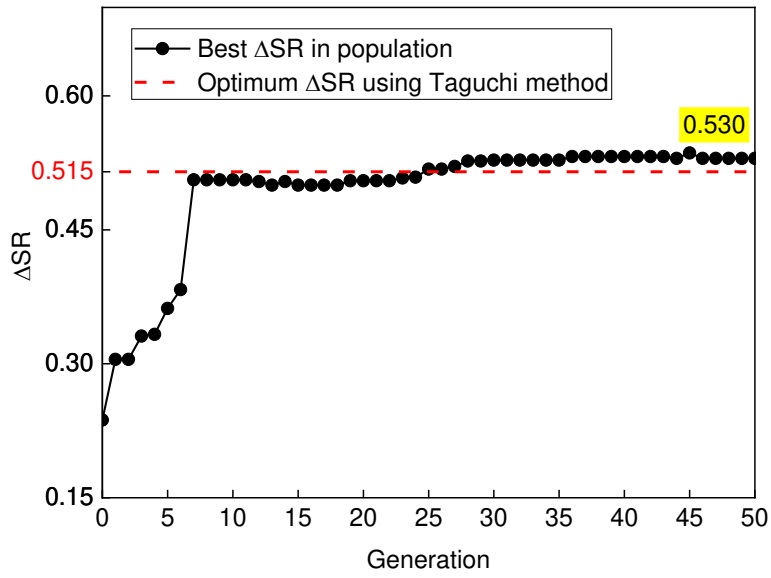

Fig. 11 Comparison of best ΔSR between the DBN5 integrated GA and Taguchi methods

List of tables

Table 1 Experimental factors and levels

Factor	Level		
	1	2	3
Particle length (mm), A	3.0	5.0	-
Particle diameter (mm), B	0.3	0.5	0.7
Particle weight (kg), C	1.0	1.4	1.8
Diluted water quantity (ℓ), D	1.0	2.0	3.0
Rotational speed (rpm), F	800	1,100	1,400
Finishing time (min), G	20	30	40

Table 2 The ratio of change in surface roughness

Exp. no.	Factor and level						ΔSR_M			
	A	B	C	D	F	G	i)	ii)	iii)	iv)
1	1	1	1	1	1	1	0.1114	0.0514	0.1199	0.1554
2	1	1	2	2	2	2	0.1415	0.0602	0.2440	0.2060
3	1	1	3	3	3	3	0.0742	0.0882	0.2892	0.2301
4	1	2	1	1	2	2	0.1278	0.0758	0.5074	0.4334
5	1	2	2	2	3	3	0.1940	0.1547	0.4818	0.5229
6	1	2	3	3	1	1	0.0574	0.0692	0.1204	0.1422
7	1	3	1	2	1	3	0.1471	0.1317	0.2884	0.3218
8	1	3	2	3	2	1	0.1203	0.1425	0.3461	0.3071
9	1	3	3	1	3	2	0.2288	0.2149	0.4218	0.4067
10	2	1	1	3	3	2	0.1296	0.0547	0.1897	0.1625
11	2	1	2	1	1	3	0.0827	0.0926	0.0876	0.0805
12	2	1	3	2	2	1	0.0392	0.0691	0.1367	0.1692
13	2	2	1	2	3	1	0.0675	0.0556	0.2524	0.2383
14	2	2	2	3	1	2	0.1739	0.1100	0.1515	0.2101
15	2	2	3	1	2	3	0.0796	0.1176	0.2931	0.2929
16	2	3	1	3	2	3	0.0642	0.1211	0.4310	0.4491
17	2	3	2	1	3	1	0.1174	0.1098	0.3686	0.3687
18	2	3	3	2	1	2	0.1518	0.0829	0.1772	0.2099

Table 3 ANOVA for multiple linear regression model

Factor	SS	DOF	V	F_0
Regression	0.09166	11	0.00833	6.27*
Residue	0.00798	6	0.00133	
Total	0.09964	17		

Table 4 Average R^2 and MSE results of DBN architectures

Architecture no.	Architecture ($\boldsymbol{v}$- $\boldsymbol{h_1}$-$\boldsymbol{h_2}$-out)	Training datasets		Testing datasets	
		R^2	MSE($\times 10^{-3}$)	R^2	MSE($\times 10^{-3}$)
DBN1	7-7-7-1	0.9797	0.3078	0.8923	1.4884
DBN2	7-7-14-1	0.9837	0.3153	0.9027	1.8651
DBN3	7-7-21-1	0.9843	0.2486	0.8970	1.6912
DBN4	7-14-7-1	0.9870	0.8710	0.8733	2.3187
DBN5	7-14-14-1	0.9900	0.1518	0.9340	1.3037
DBN6	7-14-21-1	0.9860	0.2224	0.8747	1.4972
DBN7	7-21-7-1	0.9910	0.1493	0.8813	1.8786
DBN8	7-21-14-1	0.9850	0.2344	0.9087	1.5696
DBN9	7-21-21-1	0.9787	0.3127	0.9167	1.3106

Table 5 ANOVA for training and testing datasets in DBN5

DBN5	Factor	SS	DOF	V	F_0
Training datasets	Regression	0.86491	7	0.12356	2182.43^{**}
	Residue	0.00294	52	0.00005	
	Total	0.86785	59		
Testing datasets	Regression	0.21424	7	0.03061	9.77^{*}
	Residue	0.01253	4	0.00313	
	Total	0.22677	11		

Table 6 Statistical comparison between DBN5 and multiple linear regression models

Statistical criteria	Multiple linear regression	DBN5	
		Training datasets	Testing datasets
R^2	0.9199	0.9900	0.9340
MSE	0.4432	0.1518	1.3037

Table 7 Optimal process parameters of the DBN5 integrated GA and Taguchi methods

Optimal strategy	Process parameters						
	A	B	C	D	F	G	$R_{a,initial}$
DBN5 integrated GA	3mm	0.7mm	1.3kg	1.0ℓ	1,323rpm	35min	2.478μm
Taguchi method	3mm	0.7mm	1.4kg	1.0ℓ	1,400rpm	30min	-